Flow of anisotropic ice from the EPICA core: a new test apparatus

Peter R. Sammonds,[1] S. Boon,[1] N. Hughes,[1] M. A. Rist[2]
[1]*Rock and Ice Physics Laboratory, Research School of Geological and Geophysical Sciences,*
University College London, London WC1E 6BT, England
[2]*Department of Materials Science and Metallurgy, University of Cambridge, Cambridge CB2 3Q2, England*

ABSTRACT. Our objective is to measure the mechanical properties of anisotropic ice of the EPICA ice core, from Dome Concordia, Antarctica, through the full depth of the borehole in deformation experiments under simulated ice-sheet conditions of temperature and pressure. We propose to undertake experiments on the EPICA core using both a conventional triaxial-test apparatus and a new, true, triaxial-test apparatus incorporating automated tomographic imaging of the ice-fabric evolution during deformation. We present the design of this new apparatus together with our testing methodology for EPICA ice. The new apparatus is capable of deforming an ice specimen, up to 200 mm × 100 mm × 40 mm, under servo-controlled biaxial loading with a superimposed confining pressure of 50 MPa and at temperatures down to −40°C. Highly unusual problems arising from the true triaxial nature of the apparatus and tomographic imaging are discussed.

1. INTRODUCTION

Modelling ice-sheet flow is difficult because, amongst other factors, the state of stress is not known and the flow law cannot be uniquely defined from field measurements. This arises because of (a) longitudinal deviatoric stresses resulting from bedrock and surface topography, which may be significantly larger than the shear stresses, and (b) the strongly anisotropic nature of ice flow. The first problem means that experiments on ice cores are likely to remain a significant part of any rheological investigation and second, that a properly constituted anisotropic flow law needs to be formulated. The anisotropy of polycrystalline ice, associated with anisotropic crystallographic *c*-axis orientations, results in strongly anisotropic strength. As ice is buried in an ice sheet and moves along a flowline, its degree of anisotropy changes and so does its strength. The European Project for Ice Coring in Antarctica (EPICA) is an important opportunity for investigating the flow of anisotropic ice.

Laboratory deformation experiments on Greenland and Antarctic deep-core ice have employed uniaxial compression and tension, simple-shear and conventional triaxial-compression tests (e.g. Russell-Head and Budd, 1979; Shoji and Langway, 1985; Raistrick, 1996). However these tests only allow the flow of ice to be investigated under simple-stress configurations and cannot be used to test a general anisotropic flow law. What are required are tests involving combined stresses. One such test combines direct shear and uniaxial compression (Li and others, 1996). What we have done is design a new, true, triaxial-test apparatus as this allows general axial loading configurations. The apparatus, described below, consists of biaxial loading with a superimposed confining pressure. The design uniquely incorporates automated tomographic imaging of the ice-fabric evolution

during deformation using multiple *P* and *S* elastic-wave velocity measurements.

True triaxial rigs for ice deformation have used cubic specimens loaded by three pairs of orthogonal actuators (Häusler, 1983; Gratz and Schulson, 1997). However serious doubts remain about the non-uniform nature of the stress field in such a squat specimen. Mogi (1967) on the other hand developed a combined biaxial rig and pressure vessel for rock mechanics capable of operating under compression and extension. This apparatus has the advantage of the conventional triaxial cell in using a slender specimen. We have chosen to follow this approach even though it has been technically demanding due to the low temperatures and large specimen size needed. The disadvantage of using a slender specimen is that for certain specimen orientations cut relative to the ice fabric, buckling may occur.

2. FLOW LAWS FOR ICE

Ice naturally occurring on Earth, ice 1h, has a hexagonal crystal structure with five non-zero elastic constants (Table 1). Polycrystalline ice with random crystal orientation is elastically isotropic and exhibits an average of the single-crystal response, which in itself only departs by a small amount from being elastically isotropic (Hobbs, 1974). By contrast the plasticity of ice is highly anisotropic. The easy-slip plane is the basal plane, in which there is no preferred slip direction (Kamb, 1961), but the resistance to shear on non-basal planes is considerably greater (Duval and others, 1983). Deformation of polycrystalline ice is accompanied by crystallographic lattice rotation, grain-boundary migration and dynamic recrystallization so that initially isotropic ice will develop an anisotropic fabric (cf. Castelnau and others, 1996.)

Glen (1955) showed from uniaxial-deformation tests on isotropic, laboratory-grown fresh-water ice that the flow of

1

Component	Stiffness
	GPa
C_{11}	13.2
C_{12}	6.7
C_{13}	5.8
C_{33}	14.4
C_{44}	2.9

Note: $C_{11} = C_{22}$; $C_{13} = C_{23}$; $C_{44} = C_{55}$; all other $C_{ijkl} = 0$.

ice could be described by the power creep equation. To apply Glen's law to ice-sheet modelling it was necessary to generalize the flow law in terms of stress and strain-rate invariants, which are invariant to rotation of the coordinate system. The stress invariants are: $J_1 = P$, $J_2 = 1/2 \, \mathrm{tr}(s_{ij}^2)$, $J_3 = \det s_{ij}$. P is pressure and s_{ij} is the deviatoric stress. Glen wrote the general form of the flow law assuming isotropy and incompressibility (Paterson, 1994):

$$\dot{\varepsilon} = B(J_2, J_3)s_{ij} + C(J_2, J_3)[s_{ik}s_{kj} - 2/3 J_2 \delta_{ij}].$$

It is widely assumed that the flow of isotropic ice depends only on J_2, in which case the familiar tensor flow equation of Nye (1957) can be used. However this assumption has not yet been adequately tested experimentally.

Considerable effort has gone into developing flow laws for ice relating the development of anisotropic ice fabrics to stress states and cumulative strain. Azuma and Higashi (1985) showed that ice-fabric development in shallower parts of an ice sheet, where recrystallization could be disregarded, could be modelled by *c*-axis rotation caused by basal-slip deformation. Alley (1988) extended the *c*-axis rotation model to uniaxial extension, pure shear and simple shear and modelled fabric development for each loading condition. Lliboutry (1993) observed that ice fabrics in an ice sheet have rotational symmetry about a single preferred-orientation direction, that is they are transversely isotropic, and therefore developed a constitutive relation for transversely isotropic ice. Castelnau and others (1996) developed an anisotropic visco–plastic self-consistent approach for predicting texture development. Azuma (1994) proposed an anisotropic flow law under uniaxial compression, taking into account interaction between grains, that operates with a geometric tensor incorporating the mean Schmid factor, which characterizes the mean orientation angle of the crystallographic *c* axes of ice grains with respect to the vertical. Svendsen and Hutter (1996) have proposed the use of a "macroscopic" orientation-distribution function, assuming that large-scale fabric development leads to transversely isotropic material behaviour.

However, there are few experimental studies of ice deformation under complex stresses against which to test these models. It is for this reason that we have designed the new pressurized biaxial-deformation cell for ice. As a common component of recent models is that they incorporate some orientation-distribution function to describe ice-fabric evolution, we are developing the automated tomographic-imaging system to measure fabric evolution contemporaneously with deformation.
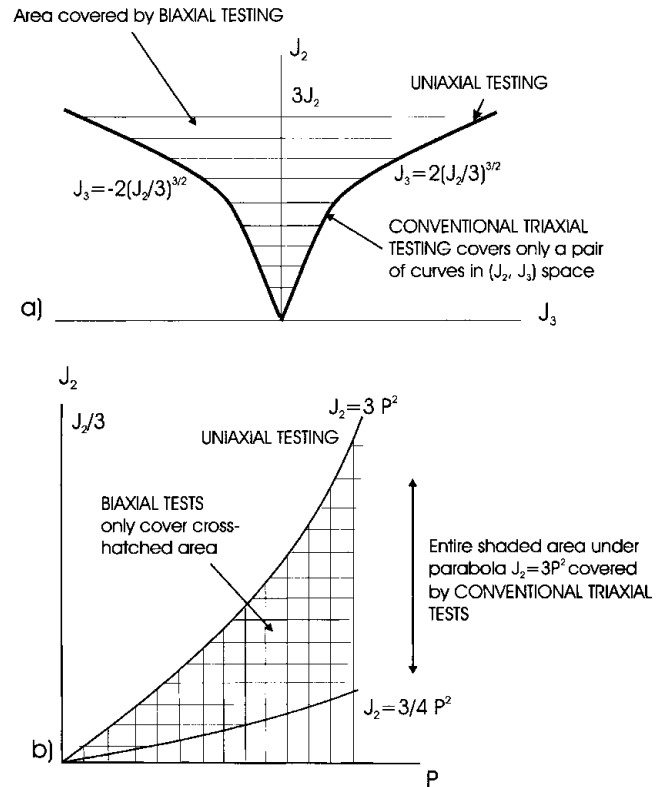

Fig. 1. Stress-invariant domains for compressive stress for: (a) (J_2, J_3) space; and (b) (P, J_2) space (after Morland and Earle, 1983). Comparison of biaxial tests ($\sigma_1 \neq \sigma_2$, $\sigma_3 = 0$) with convention triaxial tests ($\sigma_1 \neq \sigma_2 = \sigma_3$) for isotropic deformation.

3. TEST LOADING CONFIGURATION

When considering the design of a new test apparatus it is important to compare the effectiveness of different loading systems in determining the general multiaxial-loading response of ice. This has not been done for anisotropic deformation, but Morland and Earle (1983) have done this analysis for isotropic deformation, which is summarized in Figure 1. In uniaxial tests only σ_1 may be varied independently and $\sigma_2 = \sigma_3 = 0$. For true triaxial tests, all three principal stresses can be varied independently ($\sigma_1 \neq \sigma_2 \neq \sigma_3$). The conventional triaxial test is when $\sigma_1 \neq \sigma_2 = \sigma_3$, giving transversely isotropic stress. ($\sigma_2 = \sigma_3 = p$, where p is the confining pressure.) In extension tests done in the conventional triaxial cell, the axial stress, σ_1, is much less than the confining pressure. In biaxial tests, σ_1 and σ_2 may be varied independently and $\sigma_3 = 0$. Morland and Earle (1983) compare stress-invariant domains for various loading systems. In (J_2, J_3) space conventional triaxial testing is confined to a pair of curves. The effect of the intermediate principal stress may only be gauged by comparing tension and compression tests. By contrast, in the biaxial test for any given J_2, there is a range of possible values of J_3. In (P, J_2) space the conventional triaxial test provides better coverage. True triaxial testing covers the entire bound space.

True triaxial-test apparatuses are difficult to build, and tests are difficult to perform. Therefore a successful strategy for testing multiaxial flow laws would be to do experiments both in a biaxial apparatus and conventional triaxial apparatus. This presents two major problems. (1) Ice is an exceptionally brittle material (its fracture toughness is around

only 0.1 MPa m$^{1/2}$) and at high strain rates deformation is accompanied by cracking. However low stress, low strain-rate tests require long tests. It is noticeable that in some testing programmes steady-state creep has not been achieved and only transient creep measured. So it is necessary to impose a confining pressure to suppress cracking if a comprehensive test programme is to be completed in reasonable time. (2) For deep ice cores, air hydrate transforms to air bubbles when ice specimens are taken up to atmospheric pressure. These may lead to cracking. Therefore it is important to test ice-core specimens under in-situ pressure conditions.

Steady-state flow laws obtained from laboratory experiments, both in rock and ice mechanics, have been used to extrapolate laboratory measurements over many orders of magnitude of strain rate to infer lithospheric and glaciological conditions. This raises two problems. (1) Steady-state deformation frequently is not achieved during tests (e.g. Castelnau and others, 1998). (2) Even when steady-state deformation is achieved, assumptions still have to be made about the validity of the extrapolation. A newer approach has been described for geological materials by Covey-Crump (1988) which addresses both of these problems. This involves the measurement of a mechanical-state variable, which does not make the steady-state approximation. The methodology holds out great promise for ice mechanics.

4. DETERMINING FABRIC ORIENTATION BY ELASTIC-WAVE-VELOCITY MEASUREMENTS

Determining the evolution of the anisotropic ice-fabric syndeformational is an important goal. We intend to do this by measuring elastic-wave velocities for the P wave and two polarization of the S wave, $S1$ and $S2$, in three orthogonal directions to the specimen (1, 2, 3). This approach is possible because of the small but measurable elastic anisotropy in the stiffness, C_{ijkl}, of ice (Table 1). Single crystal ice lh has maximum P wave velocity, V_P, along the c axis of 4.11 km s^{-1} at 0.001 MPa and $-32°$C (Nanthikesan and Shyam Sunder, 1994). The velocity distribution is axially symmetric about the c axis because of the hexagonal symmetry. The V_P minimum is 3.84 km s^{-1} at about 45$°$ to the c axis. The V_P anisotropy is 6.9%. The shear-wave splitting anisotropy is 15%, with a maximum at about 45$°$ to the c axis. So from a combination of P- and S-wave measurements the orientation of a single-crystal c axis can in principle be determined. Wave-velocity measurements have been used in the field to measure fabric anisotropy (Bentley, 1972) and in our laboratory where P-wave velocity changes with deformation have been measured in the conventional triaxial test (Raistrick, 1996).

The determination of fabric orientation for ice by elastic-wave-velocity measurements has not been solved analytically, and in itself will be a matter for investigation during the course of our research. In Appendix 1, we outline the basic theory that has informed our apparatus design, following the development of Nikitin and Chesnokov (1981). We treat the case of hexagonal symmetry, which is applicable to the ice single crystal and ice fabric, if transverse isotropy is assumed. We find that the measurement of V_{P3}, V_{P1}, $V_{(S1)3}$, $V_{(S1)1}$ gives all five independent elastic constants. But only three wave-velocity measurements (e.g., P and $S1$ and $S2$ in one direction) need be measured to determine the orientation of the c axis of the ice single crystal.

Treating the polar ice fabric as having transverse isotropic symmetry is a reasonable assumption, and in accordance with other fabric studies in rock mechanics (Mainprice and Humbert, 1994) and in glaciology (Lliboutry, 1993). If we wish only to determine the simple c-axis maximum fabric, again only three wave-velocity measurements would be needed. General triaxial stressing imposes orthorhombic
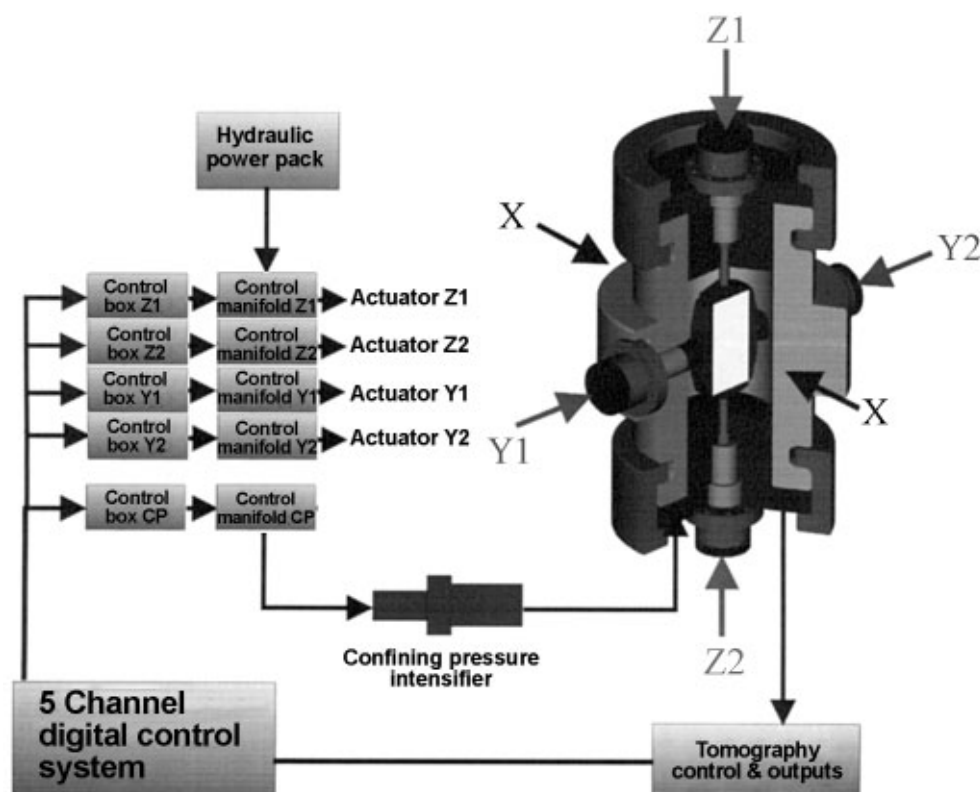

Fig. 2. Schematic diagram of the pressurized biaxial cell for ice and conceptual diagram of the loading system.

3

symmetry and more wave-velocity measurements would be needed. Under stress, four measurements of both V_P and V_S are needed to obtain the nine constants. However a complete analytical solution to this problem does not exist.

The experiment also requires making sufficient wave-velocity measurements so that averaging over the specimen is adequate. It is necessary to scan the specimen so that sufficient numbers of grains can be sampled to generate a representative crystallographic preferred orientation (on the grounds that any one elastic-wave-velocity measurement in a transversely isotropic material will yield an angular separation between the measurement direction and the c axis, for a fabric that is reasonably well-defined). It is good practice to require 300 grains for any averaged microstructural measurement (e.g. grain-size, c-axis orientation; Covey-Crump, 1997). For ice this is mitigated by the fact that it develops a simple c maximum fabric. Our typical polar ice specimen may be 160 mm × 80 mm × 30 mm in size, with a typical grain-size of say 5 mm × 5 mm × 10 mm, the specimen would contain 1500 grains. Of course there are other problems to be considered, but the specimen-size/grain-size ratio is adequate, so the sampling then becomes a question of the number of measurements needed as the specimen is scanned.

5. PRESSURIZED BIAXIAL CELL FOR ICE

A schematic diagram of the pressurized biaxial and tomographic mapping cell for ice is shown in Figure 2. The cell consists of a thick-walled pressure vessel on which are mounted four servo-hydraulic 60 kN actuators loading an ice specimen in the y and z directions with fluid-confining pressure providing the x component of stress (essentially this is a biaxial-loading rig inside a pressure vessel). Ports are available to incorporate two further actuators in the x axis. Extensional loads can be applied by attaching the specimen to the piston ram ends with epoxy resin (Mogi, 1967). The cell is capable of operating at confining pressures up to 50 MPa, temperatures down to −40°C, strain rates in the range $10^{-4}\,s^{-1}$ to $10^{-8}\,s^{-1}$ and allow strains up to 30%. The ice specimen is up to 200 mm × 100 mm × 40 mm in size, but typical specimens would be smaller. Differential stresses up to 25 MPa could be applied to a typical specimen. The entire apparatus is located inside a large cold-room complex.

The temperature range was chosen to encompass a large part of the temperature range of natural ice on Earth, while still allowing the use of a liquid-confining medium. The pressure range encompasses the pressures in ice sheets and is anticipated to eliminate cracking. The specimen size allows full use of ice-core material from the current deep-drilling programmes in Antarctica and Greenland and is sufficiently large to provide a reasonable grain-size/specimen-size ratio. In a granular test, specimen surface grains are not so confined as grains in the bulk. Unless the number of surface grains is statistically small, specimen strength will depend on the grain-size/specimen ratio. Jacka (1994) has shown that this requirement is not nearly so severe for plastic deformation of ice. Mogi (1967) found, for brittle faulting in rocks, that if the specimen-height/thickness ratio was greater than 3:3.5, the fault formed parallel to the intermediate principal stress and remained mostly in the central part of the specimen. The strength was also independent of the height/width ratio. These are strong indications that end effects at the top and bottom were probably eliminated. The strain-rate range

was chosen as the optimum for a comprehensive testing programme on ice cores. Changing to a servo valve with a different flow rate would change the strain-rate range available.

5.1. Loading system

The loading system is shown conceptually in Figure 2. The confining fluid (either low-temperature oil or alcohol) is provided by a servo-hydraulic pressure intensifier. Pressure is controlled during deformation. The specimen can be contained in a polymer jacket to keep out the confining fluid when cracks are present in the ice. However this may not be necessary for plastic-deformation tests on ice at low confining pressure using a viscous-liquid confining medium.

Four 60 kN servo-hydraulic actuators, integral to the cell, apply the load on the y and z axes. The reaction for the z actuators is taken, via the closures and clamps, by the pressure vessel. The reaction for the y actuators is taken via an integral reaction ring on the vessel. The actuators apply load to pressure-balanced pistons, which in turn load the specimen. The confining fluid is vented above a shoulder on the piston so that, as confining pressure is increased, the specimen is loaded hydrostatically. The actuators only have to provide the differential load, thereby greatly reducing their size and increasing the accuracy of load measurement. Tests can be done at constant load or displacement rate. Internal force cells in the piston-ram ends measure load, a pressure transducer measures pressure and internal and external displacement transducers (LVDTs) measure deformation. A five-channel controller, assembled from commercially available digital control cards, controls the system.

5.2. Pressure-vessel design

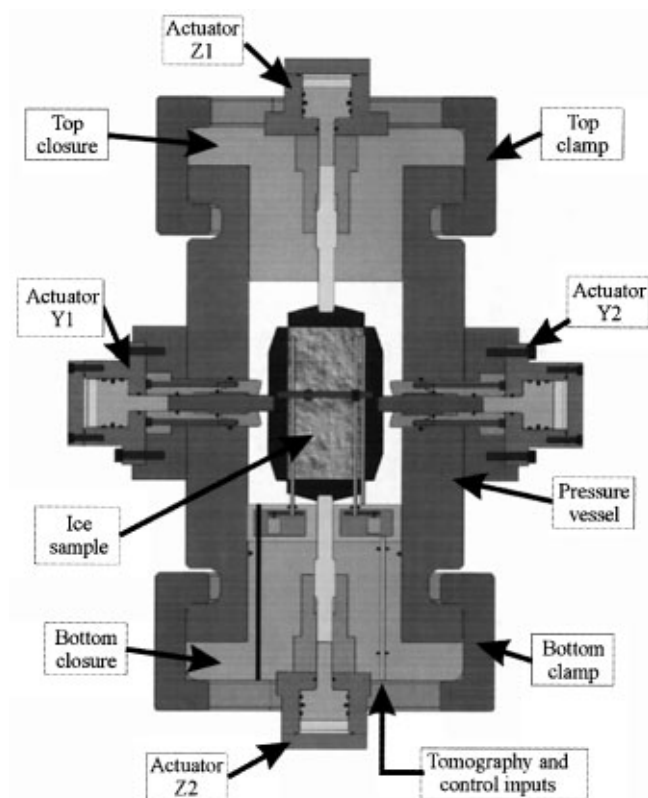The pressure vessel is a thick-walled steel monobloc cylinder

Fig. 3. Section through the pressure vessel of the pressurized biaxial cell for ice.

360 mm in diameter by 620 mm long, with an internal bore of 200 mm, designed for a maximum operating pressure of 50 MPa and minimum operating temperature of −40°C. A section is shown in Figure 3. The end loads due to the confining pressure are taken by top and bottom closure plugs secured by quick-release clamps to the vessel. Seals used are Busak and Shamban "Turcon" coated silicone "o" rings. Vessel-wall thickness is determined by the requirement to take the reaction from the clamps through to the vessel wall by an integral flange. Sammonds and others (1991) discuss the particular problems of low-temperature pressure-vessel design. Analytical equations for pressure-vessel stress analysis are given in standard texts such as Manning and Labrow (1974) and the modern fracture-mechanics approach is described in Sammonds (1988). The maximum shear stress in the vessel wall is 82 MPa and the maximum hoop stress is 114 MPa. Safe design of pressure vessels requires that the critical crack length should be greater than the wall thickness. This can be achieved for a material with fracture toughness greater than 65 MPa m$^{1/2}$. Because of the complex shape of the vessel and integral reaction ring, we have also done a finite-element analysis of the stress. Peak stresses under the flange are above 450 MPa, however these rapidly decay. This suggests that the material fracture toughness should be greater than 130 MPa m$^{1/2}$. The 25% chrome, super-duplex, stainless-steel F55 from Special Quality Steels, England, fulfils this requirement at low temperatures as well as being corrosion resistant, which is important in a cold-room environment.

The apparatus is operated inside a temperature-controlled cold room. Additional cooling is provided by circulating refrigerants through copper tubing close wound onto the vessel from a free-standing temperature-controlled cryostat. The temperature controller uses the average output from four resistance thermometers located close to the specimen in the piston ends. The large mass of the vessel ensures the temperature stability of better than 0.2°C (Sammonds and others, 1991).

5.3. Elastic-wave-velocity measurement

Our analysis shows that only four combinations of P and two S elastic-wave polarizations are necessary to determine the c-axis maximum fabric orientation. As the research programme develops, we anticipate that we will become interested not only in determining the crystallographic c-axis orientation, but also the a and b axes, for which more wave-velocity measurements will be required.

Our design allows for P and the two S polarizations to be measured on each axis. In the y- and z-loading platens, a series of P- and S-wave transducers are embedded in the faces of the loading pistons. In the x-plane specimen surfaces a pair of pressure-wave (P) ultrasonic transducers and two pairs of orthogonal shear-wave (S) transducers scan the specimen, controlled by stepper motors. Miniature hydraulic actuators provide clamping of the transducers to the specimen. The scanning system is shown conceptually in Figure 4. P- and S-wave velocities are measured by the pulse-receive method of Birch, used in rock mechanics (Sammonds and others, 1989). Here a computer-controlled generator pulses the transmitter transducers several hundred times per minute, and the travel times to the receiver transducers are measured by timing cards and averaged. 0.5 MHz PZT transducers will be used. A full scan of the specimen surface, with some 40 plus measurement positions, take 2–3 min. These measurements will produce a spatially averaged velocity-distribution map
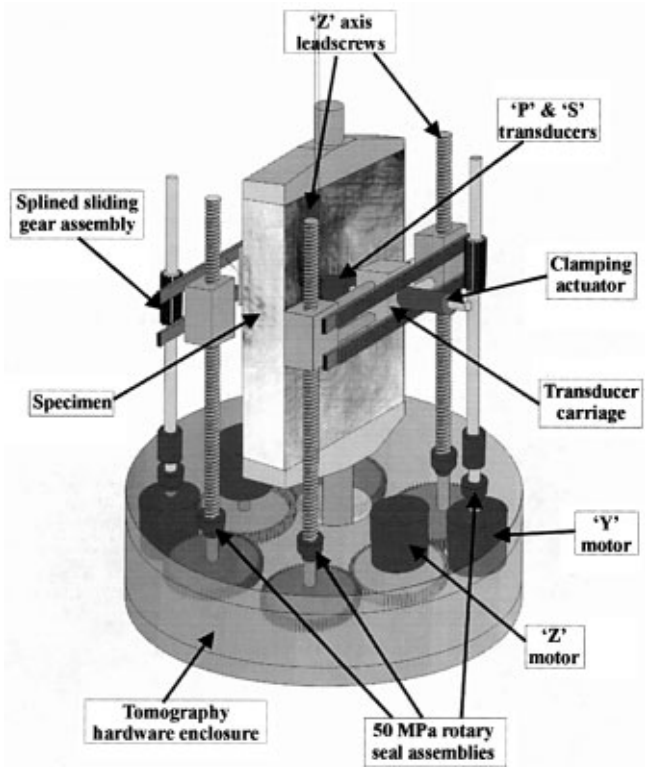

Fig. 4. Conceptual diagram of the scanning elastic-wave-velocity tomographic system.

of the specimen automatically, from which the fabric evolution can be inferred.

6. TEST METHODOLOGY

In terms of the EPICA programme our objective is to measure the mechanical properties of anisotropic ice of the EPICA ice core through the full depth of the borehole in deformation experiments under simulated Antarctic ice-sheet conditions of temperature and pressure. Four types of experiments will be done: (1) Pressurized biaxial-deformation tests allowing the anisotropic-flow properties to be measured, where the development of anisotropic c-axis orientations during deformation will be continuously monitored by the tomographic-imaging system. (2) Hydrostatic tests to measure
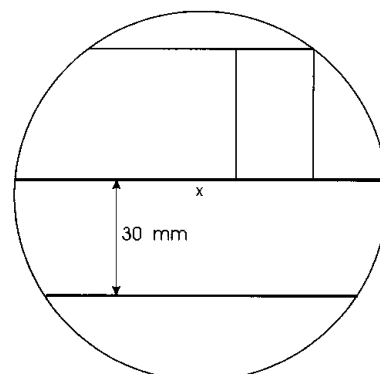

Fig. 5. EPICA–Dome C core-cutting scheme for mechanical- and physical-properties studies.

5

recrystallization kinetics. (3) Conventional triaxial-deformation experiments using specimen cut at $0°$, $45°$ and $90°$ to the vertical (to allow comparison with other laboratories). (4) Stress-relaxation tests in the pressurized biaxial cell and conventional triaxial cell to achieve very low strain rates.

The EPICA core from Dome Concordia will have a 98 mm diameter. A central section from the core will be cut for the confined biaxial-test specimen, up to 160 mm long by 80 mm wide by 30 mm thick (Fig. 5). One bag in every 200 will be cut according to this scheme. This will provide adequate samples for a comprehensive testing programme.

Initially isotropic ice at the surface of an ice sheet develops an anisotropic fabric in the prevailing stress field as it is buried and moves along a flowline, via primary and secondary creep to steady tertiary creep. Achieving tertiary creep in the laboratory takes a long time and, in an arbitrary stress field, would involve the destruction of the existing ice fabric and the evolution of a new one. However, it has been demonstrated that if the ice core is subjected to the same stress configuration in the laboratory as in the field and the fabric is not destroyed, then deformation passes straight from primary to tertiary creep (Shoji and Langway, 1985). In the confined biaxial cell, ice cores can be deformed at in-situ pressure and temperature and in a stress field compatible with its developed anisotropy. The subsequent fabric evolution can be measured by the tomographic-imaging system. The stress field then can be subsequently altered. These tests should allow anisotropic flow parameters to be measured.

ACKNOWLEDGEMENTS

REFERENCES

Alley, R. B. 1988. Fabrics in polar ice sheets: development and prediction. *Science*, **240**(4851), 493–495.

Azuma, N. 1994. A flow law for anisotropic ice and its application to ice sheets. *Earth Planet. Sci. Lett.*, **128**(3–4), 601–614.

Azuma, N. and A. Higashi. 1985. Formation processes of ice fabric pattern in ice sheets. *Ann. Glaciol.*, **6**, 130–134.

Bentley, C. R. 1972. Seismic-wave velocities in anisotropic ice: a comparison of measured and calculated values in and around the deep drill hole at Byrd Station, Antarctica. *J. Geophys. Res.*, **77**(23), 4406–4420.

Castelnau, O., P. Duval, R. Lebensohn and G. R. Canova. 1996. Viscoplastic modeling of texture development in polycrystalline ice with a self-consistent approach: comparison with bound estimates. *J. Geophys. Res.*, **101**(B6), 13,851–13,868.

Covey-Crump, S. J. 1997. The normal grain growth behaviour of nominally pure calcitic aggregates. *Contrib. Mineral. Petrol.* 129, 239–254.

Covey-Crump, S.J. 1998. Evolution of mechanical state in Carrar marble during deformation at 400°C to 700°C. *J. Geophys. Res.*, **103**(B12), 29,781–29,794.

Duval, P., M. F. Ashby and I. Anderman. 1983. Rate-controlling processes in the creep of polycrystalline ice. *J. Phys. Chem.*, **87**(21), 4066–4074.

Glen, J.W. 1955. The creep of polycrystalline ice. *Proc. R. Soc. London, Ser. A*, **228**(1175), 519–538.

Gratz, E. T. and E. M. Schulson. 1997. Brittle failure of columnar saline ice under triaxial compression: the failure surface. *J. Geophys. Res.*, **102**(B3), 5091–5107.

Häusler, F. U. 1983. Comparison between different yield functions for saline ice. *Ann. Glaciol.*, **4**, 105–109.

Hobbs, P.V. 1974. *Ice physics.* Oxford, Clarendon Press.

Jacka, T. H. 1994. Investigations of discrepancies between laboratory studies of the flow of ice: density, sample shape and size, and grain-size. *Ann. Glaciol.*, **19**, 146–154.

Kamb, W. B. 1961. The glide direction in ice. *J. Glaciol.*, **3**(30), 1097–1106.

Li Jun, T. H. Jacka and W. F. Budd. 1996. Deformation rates in combined compression and shear for ice which is initially isotropic and after the development of strong anisotropy. *Ann. Glaciol.*, **23**, 247–252.

Lliboutry, L. 1993. Anisotropic, transversely isotropic nonlinear viscosity of rock ice and rheological parameters inferred from homogenization. *Int. J. Plasticity*, **9**(5), 619–632.

Mainprice, D. and M. Humbert. 1994. Methods of calculating petrophysical properties from lattice preferred orientation data. *Surv. Geophys.*, **15**(5), 575–592.

Manning, W. R. D. and S. Labrow. 1974. *High pressure engineering.* London, Leonard-Hill.

Mogi, K. 1967. Effect of intermediate principal stress on rock failure. *J. Geophys. Res.*, **72**(20), 5117–5131.

Morland, L.W. and E. N. Earle. 1983. Correlation of shear behaviour with biaxial stress response. *In POAC 83. Seventh International Conference on Port and Ocean Engineering under Arctic Conditions, 5–9 April 1983, Espoo, Finland. Proceedings. Vol. 3.* Espoo, Finland, Valtion Teknillinen Tutkimuskeskus, 183–192.

Nanthikesan, S. and S. Shyam Sunder. 1994. Anisotropic elasticity of polycrystalline ice I$_h$. *Cold Reg. Sci. Technol.*, **22**(2), 149–169.

Nikitin, L. V. and E. M. Chesnokov. 1981. Influence of a stressed condition on the anisotropy of elastic properties in a medium. *Izv. Earth Phys.*, **17**(3), 174–183.

Nye, J. F. 1957. The distribution of stress and velocity in glaciers and ice-sheets. *Proc. R. Soc. London, Ser. A*, **239**(1216), 113–133.

Paterson, W. S. B. 1994. *The physics of glaciers. Third edition.* Oxford, etc., Elsevier.

Raistrick, D. C. 1996. Flow of Greenland ice. (Ph.D. thesis, University College London.)

Russell-Head, D. S. and W. F. Budd. 1979. Ice-sheet flow properties derived from bore-hole shear measurements combined with ice-core studies. *J. Glaciol.*, **24**(90), 117–130.

Sammonds, P. R. 1988. Triaxial deformation experiments on natural sea ice as a function of temperaure and strain rate. (Ph.D. thesis, University College London.)

Sammonds, P. R., M. A. Ayling, C. Jones, P. G. Meredith and S. A. F. Murrel. 1989. A laboratory investigation of acoustic emission and elastic wave velocity changes during compressional rock failure under triaxial stresses. *In* Maury, V. and D. Fourmaintraux, *eds. Rock at great depth. Vol. 1.* Rotterdam, Balkema, 291–296.

Sammonds, P. R., S. A. F. Murrell, M. A. Rist and D. Butler. 1991. The design of a high-pressure low-temperature triaxial deformation cell for ice. *Cold Reg. Sci. Technol.*, **19**(2), 177–188.

Shoji, H. and C. C. Langway, Jr. 1985. Mechanical properties of fresh ice core from Dye 3, Greenland. *In* Langway, C. C., Jr, H. Oeschger and W. Dansgaard, *eds. Greenland ice core: geophysics, geochemistry, and the environment.* Washington, DC, American Geophysical Union, 39–48. (Geophysical Monograph 33.)

Svendsen, B. and K. Hutter. 1996. A continuum approach for modelling induced anisotropy in glaciers and ice sheets. *Ann. Glaciol.*, **23**, 262–269.

APPENDIX 1

Following Nikitin and Chesnokov (1981), the solution for plane-wave propagation in anisotropic elastic media is given by the Green–Christoffel equation (GCE):

$$(\Gamma_{ik} - \rho V^2 \delta_{ik})u_k = 0$$

where $\Gamma_{ik} - C_{ijkl}n_j n_l$, ρ is density, V is the phase velocity, δ_{ik} is the Kroneker delta, u_k is displacement, and n_j is the direction of the wave vector. To determine the elastic-wave velocities, the GCE can be determined for any direction in the anisotropic medium. We do not consider group velocities at this stage.

For hexagonal symmetry (in matrix form according to the rule 11–1, 22–2, 33–3, 23–4, 13–5, 12–6):

$\Gamma_{11} = n^2{}_1 C_{11} + n^2{}_2 C_{66} + n^2{}_3 C_{44}$ $\Gamma_{12} = (C_{11} + C_{66}) n_1 n_2$

$\Gamma_{22} = n^2{}_1 C_{66} + n^2{}_2 C_{22} + n^2{}_3 C_{44}$ $\Gamma_{13} = (C_{13} + C_{44}) n_1 n_3$

$\Gamma_{33} = (n^2{}_1 + n^2{}_2) C_{44} + n^2{}_3 C_{33}$ $\Gamma_{23} = (C_{13} + C_{44}) n_2 n_3$

(See Table 1.) GCE has non-trivial solutions when:

$$|\Gamma_{ik} - \rho V^2 \delta_{ik}| = 0$$

For hexagonal symmetry where the plane wave is propagating in plane $OX_1 OX_3$:

$$\left[(\Gamma_{11} - \rho V^2)(\Gamma_{33} - \rho V^2) - \Gamma^2{}_{13} \right] (\Gamma_{22} - \rho V^2) = 0$$

This gives:

$$V^2{}_{S1} = \Gamma_{22}/\rho = (C_{66} n^2{}_1 + C_{44} n^2{}_3)/\rho$$

$$V^2{}_P = 1/\rho \left([\Gamma_{11} + \Gamma_{33}]/2 + \sqrt{[\Gamma_{11} - \Gamma_{33}]^2/2 + \Gamma^2{}_{13}} \right)$$

$$V^2{}_{S2} = 1/\rho \left([\Gamma_{11} + \Gamma_{33}]/2 - \sqrt{[\Gamma_{11} - \Gamma_{33}]^2/2 + \Gamma^2{}_{13}} \right)$$

The measurements of P and the two polarizations of S-wave velocities, $V^2{}_{S1}$, $V^2{}_{S2}$, along the axes of symmetry ($n_1 = n_2$; $n_3 = 1$) OX_3 lead to the determination of two elastic constants

$$C_{33} = \rho V^2{}_{P3} \qquad C_{44} = \rho V^2{}_{(S1)3}$$

For hexagonal symmetry $V_{(S1)3} = V_{(S2)3}$ and no shear-wave splitting occurs along the axis of symmetry. Measurements of P and $S1$ and $S2$ velocities in a plane of symmetry OX_1 (perpendicular to axis of symmetry) give:

$$C_{11} = \rho V^2{}_{P1} \qquad C_{66} = \rho V^2{}_{(S1)1} \qquad C_{44} = \rho V^2{}_{(S2)3}$$

In order to determine C_{13} it is necessary to measure P or S velocity in any direction $\varphi = \varphi^0$ (not parallel or perpendicular) to the axis of symmetry. In this case from GCE, C_{13} can be calculated:

$$C_{13} = 1/n_1 n_3 [(\rho V^2{}_P(\varphi^0) - (A1)^2 - (A2)^2]^{1/2} - \rho V^2{}_{(S1)3}$$

where: $n_1 = \sin(\varphi^0)$; $n_3 = \cos(\varphi^0)$;

$$A1 = 1/2 [(\rho V^2{}_{P1} n^2{}_1 + V^2{}_{P3} n^2{}_3 + \rho V^2{}_{(S1)3}];$$
$$A2 = 1/2 [(\rho V^2{}_{P1} n^2{}_1 - V^2{}_{P3} n^2{}_3) + \rho V^2{}_{(S1)3} (n^2{}_3 - n^2{}_1)].$$

The measurements of V_{P3}, V_{P1}, $V_{(S1)3}$ and $V_{(S1)1}$ give all five independent elastic constants. But only three wave-velocity measurements (e.g. P and $S1$ and $S2$ in one direction) need measured to determine the orientation of the c axis of the ice single crystal.